Contents lists available at ScienceDirect

Electrochimica Acta

A microelectrochemical scanning flow cell with downstream analytics

Sebastian Oliver Klemm[a], Janine-Christina Schauer[b], Bernd Schuhmacher[b], Achim Walter Hassel[a,c,*,1]

[a] *Max-Planck-Institut für Eisenforschung GmbH, Max-Planck-Str. 1, 40237 Düsseldorf, Germany*
[b] *Dortmunder OberflächenCentrum, Eberhardstr. 12, 44145 Dortmund, Germany*
[c] *Institute for Chemical Technology of Inorganic Materials, Johannes Kepler University, Altenberger Str. 69, 4040 Linz, Austria*

ABSTRACT

The combination of a capillary based microelectrochemical flow cell system and downstream UV–vis analytics allows obtaining synchronized electrochemical and spectroscopic data in a fully automated mode. This method combination can be generally applied to microelectrochemical studies in which an electrochemical species is released or consumed during the electrochemical reaction. For the example of pure zinc surfaces, the characterization of the integrated spectroscopic system is presented with a Zn^{2+} detection limit below $0.1\,\mu mol\,l^{-1}$ using Zincon as complexing agent. A parameter screening of the effect of pH in the range of 6.6–9.0 in borate buffer reveals a linear increase in zinc dissolution with proton concentration but a distinct step in the open circuit potential from the active state (around $-700\,mV$ SHE, pH 6.6–7.1) to the passive state (around $-300\,mV$ SHE, pH 7.4–9.0) indicating the formation of a closed passive layer. This mechanism is strongly influenced by sulfate anions which increase the dissolution rate of the passive film and promote the active state as monitored by the dissolution profile and OCP (open circuit potential) values. Within the scope of this parameter variation, the congruency between OCP transients, potentiodynamic sweeps and time resolved dissolution profiles is discussed.

© 2011 Elsevier Ltd. All rights reserved.

1. Introduction

The importance of zinc for corrosion protection of steel is immense. Due to this, an improvement of the protective properties of zinc coatings leads to the prospect of a significant economic gain. Zinc based coatings can provide both, cathodic protection by sacrificial dissolution and the formation of passive films depending on the environmental conditions [1,2]. It is well known that zinc and zinc coatings are strongly sensitive to the surrounding conditions [3]. The parameter space solely given by the surrounding electrolyte in an aqueous environment is large and multi-dimensional. The most obvious electrolyte characteristic with immediate effect on the properties of zinc is the pH value. In 1962, Hurlen [4] found a linear relationship between logarithmic corrosion rate and pH (thus, a proportionality between current density and proton concentration) in acidic solutions in the presence of high chloride concentrations (3 M). Investigations with a ring-disc electrode on zinc performed by Boto and Williams revealed interferences of zinc hydroxide precipitation with the transport controlled oxygen reduction starting at pH values from 5.2 towards more alkaline media [5]. Powers and

Breitner provided a model for zinc passivity with different types of passive films which extends the view over a simple hydroxide precipitation [6], as supported by Chang and Prentice [7]. The strong influence of the passive layer on the electrochemical properties and the variety of precipitates in alkaline solutions were described by Hassel et al. [8,9]. However, a major challenge concerning all previous works on zinc is the comparability of studies performed in different electrolytes. The effect of pH and either aggressive or passivating anions [9,10] is seldom separately addressed. One obvious issue is that the experimental effort scales polynomially with the number of variables under individual investigation. Hence, the studies on pitting by halides [11] or film breakdown by sulfate anions [12,13] were performed in unbuffered solution at a fixed starting pH. The drawback of unbuffered solutions is that the local pH on the surface is affected by both anodic and cathodic reaction [14] as well as cathodic currents applied prior to anodic sweeps (e.g. by starting cathodically with respect to OCP) and therefore largely unknown, even though these media appear realistic concerning real corrosion processes [2].

Given the extensive amount of electrochemical data from the literature, the link to the application oriented point of view with focus on long term corrosion and real mass loss over time is still not fully achieved.

Facing this challenge, it appears useful to monitor the dissolution of zinc in parallel to all electrochemical experiments and to describe the correlation between the real time dissolution and the electrochemical data obtained. Furthermore, the investiga-

---

* Corresponding author at: Institute for Chemical Technology of Inorganic Materials, Johannes Kepler University, Altenberger Str. 69, 4040 Linz, Austria. Tel.: +43 732 2468 8704; fax: +43 732 2468 8905.

E-mail address: hassel@elchem.de (A.W. Hassel).

[1] ISE active member.

tion of different experimental parameters benefits greatly from an improvement of the experimental throughput. The aim of the work presented here is to demonstrate the feasibility of a combined high throughput microelectrochemical cell and real time monitoring of zinc dissolution by UV–vis spectroscopy. Experiments performed focus on the passivation behaviour of zinc in borate buffer [15] at pH values between 6.6 and 9.0 and the effect of small additions of sulfate anions thereon. This is a very timely issue as can be seen from the fact that results from parallel efforts to link electrochemistry on Zn alloys with downstream analytics [16] became available during the editorial process of this manuscript.

2. Experimental

2.1. Sample preparation and electrolytes

A 2 cm × 2 cm piece of 2 mm thick zinc foil of 99.99% purity (Alfa Aesar GmbH & Co KG, Karlsruhe, Germany) was ground with Si–C grinding paper (200–4000 grit) and finally polished with a 20 nm SiO_2 nanoparticle suspension. The surface was repeatedly washed with ethanol (p.a. grade, Merck KGaA, Darmstadt, Germany) and ultrapure deionised water (PureLab Plus, Elga, Celle, Germany) and finally blow dried with argon.

Electrolytes used in this study were prepared from ultrapure water and 0.1 M boric acid (p.a. grade, Merck) and the pH adjusted by addition of 0.1 M sodium hydroxide (1 M for pH 9.0 respectively) solution under stirring and pH monitoring using a glass electrode (E-632 Digital pH-Meter, Metrohm AG, Herisau, Switzerland). This electrolyte will be referred to as 0.1 M borate buffer since the sum of the concentrations of boric acid and sodium borate equals $0.1 \, mol \, l^{-1}$.

2.2. Atomic force microscopy

Atomic force microscopy was carried out on a JPK NanoWizard AFM (JPK Instruments AG, Berlin, Germany) operating in contact mode with a silicon cantilever (CONTR obtained from BudgetSensors, typical tip radius <10 nm). 10 μm × 10 μm topography scans were performed on the polished zinc sample and selected spots after the electrochemical measurements and the roughness evaluated by cross section analysis.

2.3. Flow type scanning droplet cell (f-SDC)

The flow type scanning droplet cell was built using a theta-capillary based concept [17]: a theta capillary of 1.5 mm diameter and a wall thickness of 100 μm (World precision instruments, Berlin, Germany) was heated and pulled using a PC-10 capillary puller (Narishige, Tokyo, Japan). The resulting tip was ground (EG-400 grinder, Narishige, Tokyo, Japan) to give an opening diameter around 200 μm. Mechanical removal of the separating inner wall at the very tip provided a pathway for the electrolyte to stream from one compartment of the capillary into the other. A silicone gasket to seal the wetted area during contact with the substrate was prepared by dipping the tip into RTV 118Q acetoxy curing silicone (Momentive, New York, USA) and maintaining a steady flow of nitrogen through the tip during the curing process. Fig. 1 shows an optical image of the tip used in this study from the side view.

The size of the wetted area was determined by optical analysis of Ta_2O_5 grown on a Ta thin film as described elsewhere [18] and found to be 65,210 μm^2. After tip preparation, a μ-Ag/AgCl micro reference electrode and the electrolyte supply channel was inserted into one compartment of the capillary. The reference electrode used in this study was made from 100 μm Ag-wire (99.999%, Wielandt Dentaltechnik, Germany) inside a 350 μm micro capillary (World Precision Instruments, Berlin, Germany) polarised and
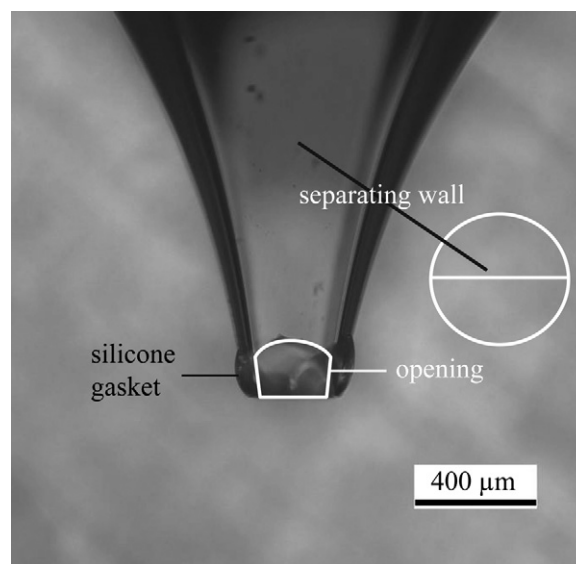

Fig. 1. Optical image of the capillary tip, side view, perpendicular to the plane of the separating wall.

tested according to Ref. [19]. The other compartment holds the counter electrode made from flattened 50 μm Pt-wire (99.99%, Goodfellow, Bad Nauheim, Germany) and the electrolyte drain being a 350 μm micro capillary as used for the reference electrode. The area of the counter electrode exceeded the wetted area by at least a factor of 10. In order to minimize the dead volume of the cell, both the counter electrode and the drain-capillary were put in close proximity to the tip, whereas the geometry was carefully adjusted to ensure proper and sustained wetting of the Pt-wire. Tubing attached to the cell were tygon® silicone tubes of 2 mm outer and 0.38 mm inner diameter (VWR international GmbH, Darmstadt, Germany) providing the connection to a REGLO digital MS-4/12-100 peristaltic pump which works both, the electrolyte flow and provides a stream of complexing agent to be mixed with the drained electrolyte in a Y-connector prior to UV–vis spectroscopic analysis. The pumping speed was set to 2 rpm which translates into $15.6 \, \mu l \, min^{-1}$ as determined by calibration with ultrapure water and a precision micro scale. Fig. 2 schematically shows the setup described.

The mechanics around the microcell consists of a xy-translation stage (M-403.6 DG, Physik Instrumente, Karlsruhe, Germany) and a KD45 2N force sensor (ME-Messsysteme, Hennigsdorf, Germany) which provides accurate sample positioning (sub μm accuracy) and accurate force readings (±0.02 mN) when in contact mode. The applied force was set to 30 mN and was constantly regulated during measurement with a frequency around 1 Hz by a feedback loop with the z-positioning system (M-227 DC Motor, Physik Instrumente, Karlsruhe, Germany). An in-house developed LabView program controls all instruments including an IviumStat potentiostat (Ivium Technologies, De Zaale, The Netherlands) and automatically saves all data obtained.

2.4. UV–vis spectroscopy

A StellarNet EPP 2000 (StellarNet Inc., Tampa, USA) spectrometer using a 2048 pixel OMA (optical multichannel array) with 300 μm fiber optics was equipped with a SL-1 Tungsten Halogen lamp with a wavelength range from 350 to 2300 nm. A custom made acrylic block with drilled channels of 400 μm in diameter following a Z-geometry was used as a flow cell with 10 mm path length.
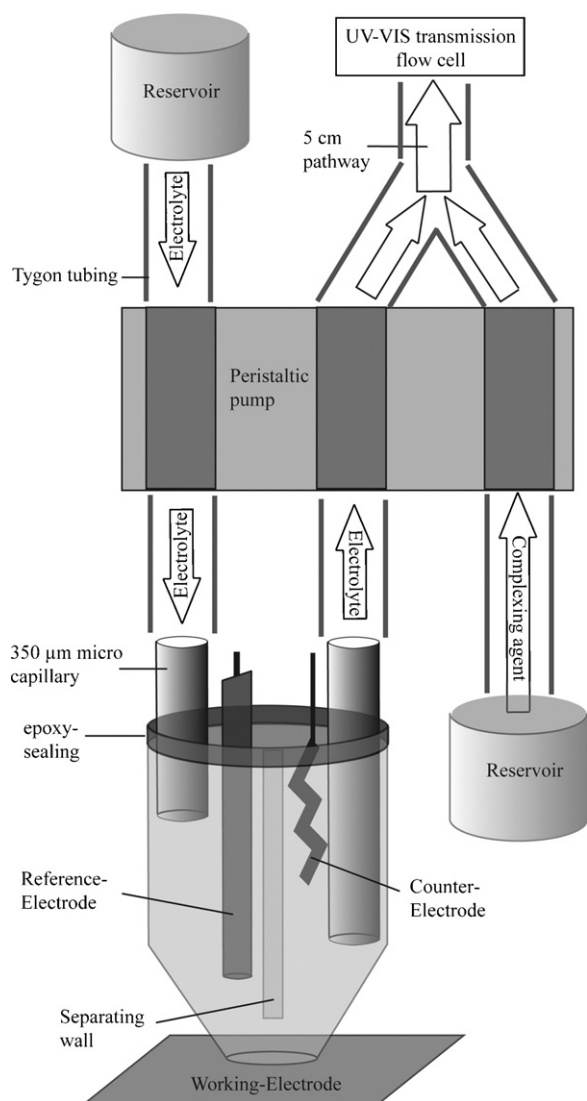
Fig. 2. Schematic drawing of the flow type scanning droplet cell.

Acquisition of the whole spectrum was executed by Lab-View and processed as a two-dimensional array. At two chosen wavelengths, the arithmetic mean was taken along ±5 nm post acquisition and the difference in absorption calculated. A set of spectra plotted for different zinc concentrations showed an isos-bestic point, which is a clear proof for a simple kinetics without follow-up reactions in the formation of the coloured zinc complex. Two points were chosen as the wavelength of maximum absorption of the complexing agent (580 nm) and at 845 nm, a point which remains unaffected by the complexing process both having the same intensity in the emission spectrum of the light source (845 nm). This procedure ensures that small intensity changes, for example refraction caused by a joint of two density fronts in the electrolyte, are not misinterpreted as a complexing process.

Furthermore, the intensity at 845 nm is taken as the reference to identify possible disturbances. A very common problem is the presence of tiny gas bubbles that occasionally stick in the pathway of the light beam, causing a massive drop in intensity. If the LabView program recognizes intensity drops of more than 10% at 845 nm lasting for at least 30 s, a short but intense stream of water is injected into the system by a Micro 4 syringe controller (World precision instruments, Berlin, Germany) with a 500 μl syringe to flush

the flow-cell. This process obviously disturbs an ongoing detection and needs to be corrected afterwards.

Since all spectroscopic data obtained is complementary to elec-trochemical processes, a transformation of detected concentration and corresponding current [20] can be obtained by multiplication of the detected concentration $c\,(\mathrm{mol\,l^{-1}})$ with the flow rate $f\,(\mathrm{l\,s^{-1}})$, the number of electrons transferred from each metal ion z and the Faraday constant $F\,(C\,\mathrm{mol^{-1}})$ according to the following formula:

$$i_{\mathrm{Zn}} = f \cdot c \cdot z \cdot F \tag{1}$$

The resulting current can further be expressed as a current density to allow direct comparison between electrochemical and spectroscopic data.

2.5. Complexing agent

A pH 9.25 200 μmol^{-1} solution of Zincon (2-carboxy-2′-hydroxy-5′-sulfoformazyl-benzene sodium salt, Merck KGaA, Darmstadt, Germany) was prepared by dissolving the required amount in a solution of 0.1 M di-sodiumtetraborate in ultrapure water. The solution was kept in the dark and injected into the flow system through the peristaltic pump. The diameter of the pump tubing was 0.19 mm which leads to a 1:4 ratio between complex-ing agent and analyte (pumped by 0.38 mm tubing, see Section 2.3) to minimize the added volume by the complexing agent and therefore minimize the dilution of the analyte. The pH of 9.25 was chosen because of the high stability of the Zincon–zinc complex at the resulting pH value [21].

2.6. Electrochemical measurements

Potential Sweeps were performed with a scan rate of 2 mV s^{-1} and a step size of 0.25 mV starting at the previously recorded OCP (1000 s). Anodic and cathodic directions were swept separately and the $[\mathrm{Zn}^{2+}]$ concentration was continuously measured. A new posi-tion on the zinc surface was used for each individual measurement, whereas the cell was kept in air for 800 s with continued flow in between to ensure complete removal of all dissolution products.

3. Results and discussion

3.1. System parameters

The following spectroscopic characteristics of the UV–vis sys-tem used in this study have been determined:

The dead time as the time lag between a dissolution event at the tip and the detection via UV–vis was calculated from gal-vanostatic dissolution steps in 0.04 M HCl on pure Cu (thermally evaporated on a silicon wafer according to [22]) and the peak posi-tion on the time axis with respect to the induced dissolution. Fig. 3 shows the recorded absorption transients during the experiment on two different spots on the copper substrate to demonstrate repro-ducibility. Copper was superior to zinc in this experiment because of the ability to form stable Cu–Zincon complexes in combina-tion with the absence of corrosion at the rest potential. A value of $t_{\mathrm{d}} = 157$ s was found for a pumping speed of 2 rpm or 15.6 μl min^{-1} respectively.

The proportionality factor between absorption and concen-tration was calculated from the slope of the absorption vs. concentration diagram recorded by immersing the cell into dif-ferent standard solutions (prepared from p.a. grade zinc sulfate, Merck). This value was found to be 81 counts/μmol l^{-1}. It is to men-tion that the calibration is only valid for a given pumping speed since the time allowed for formation of the complex in the tubing scales inversely with the pumping speed. Therefore, the pumping speed was exclusively kept at 2 rpm.
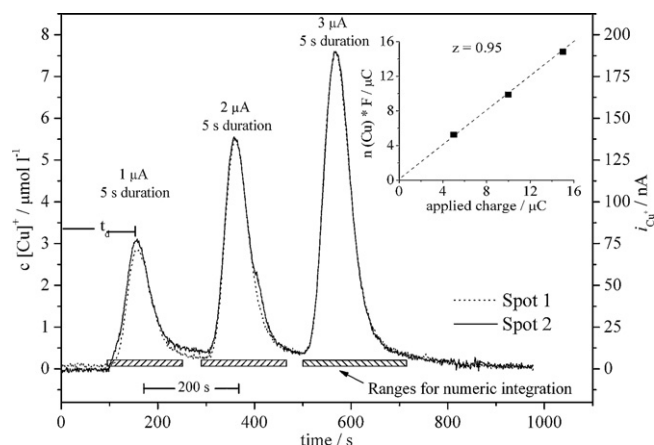
Fig. 3. Recorded absorption (580 nm) during galvanostatic dissolution steps on pure copper. Two measurement series are shown.

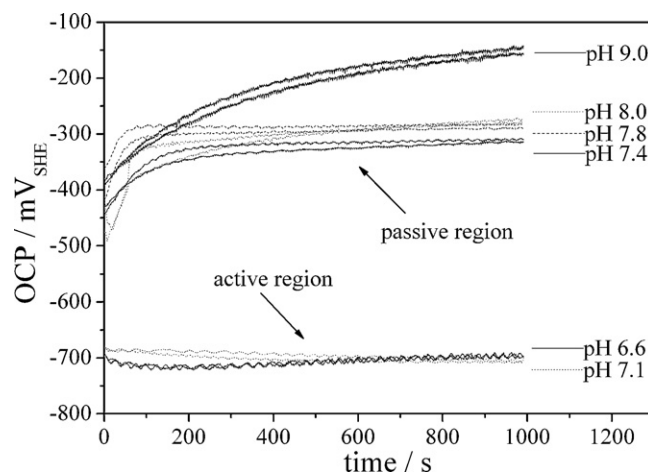**Fig. 5.** Corrosion potential transients of pure zinc in 0.1 M borate buffer at different pH values.

As mentioned in Section 2.4 and Eq. (1) in particular, the detected copper concentration can be transformed into a current signal by the equation mentioned using a copper valence of $z = 1$. Direct comparison of the detected copper ions (numerically integrated from the dissolution profile as indicated in the Figure) multiplied with the Faraday constant and the applied charge reveals a linear relationship with a slope of 0.95 which is in good agreement with the assumed valence of 1 and consistent with the values found by Ogle and Weber [20].

The topography of the surface was determined by AFM after 3 h OCP measurement on zinc in pH 6.6 buffer. The area of inspection was the boundary area at the silicone sealing to estimate possible inhomogeneities concerning the removal of zinc or crevice effects. As shown in Fig. 4, the removal of zinc appears very even since the plateau value around $-4\,\mu m$ is reached within a few μm distance with respect to the sealing. This homogeneous removal is in agreement with the results obtained by Lohrengel et al. on iron [17].

3.2. The effect of pH

3.2.1. OCP measurements

The open circuit potentials measured at different pH values are shown in Fig. 5. Two measurements are shown for each pH value to allow estimation of the reproducibility. Foremost, it can be observed that the OCPs exhibit values of around 500 mV spread within the pH window between 6.6 and 9.0. This magnitude

requires a surface change to take place since pH induced shift of the cathodic and anodic half cell reactions cannot account for the observed behaviour [4]. Furthermore, this sudden change can be localized between pH 7.1 and 7.4, with only minor increases of the corrosion potential with pH before and thereafter. At a pH value of 9.0, unlike all other measurements, the OCP did not stabilize within the duration of the experiment. This can be attributed to the very low solubility of zinc hydroxide in this pH region leading to ongoing precipitation nearly unaffected by the convection present [23]. Even though absolute values of open circuit potentials on zinc cannot be decomposed to draw conclusions about precise electrochemical reactions, the major change located between pH 7.1 and 7.4 can be associated with the dominant process concerning the OCP in the pH value under investigation. Since these values are not area dependent, the described step is assumed to indicate a close coverage of the active zinc surface by a barrier layer [23] at which the potential switches from a direct dissolution to a corrosion through this layer.

3.2.2. Polarisation curves

This mechanism is further supported by the potential sweeps subsequent to the OCP measurements as shown in Fig. 6. A pH value of 7.1 exclusively shows the pre-passivation peak (A) at $-410\,mV$ (SHE) indicating a transition from an active to a passive surface
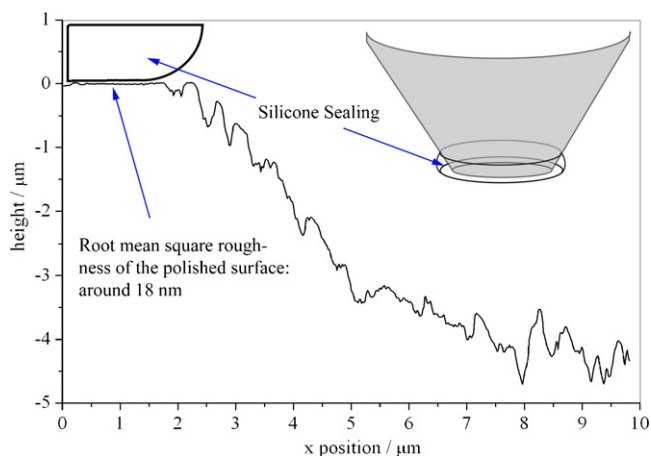
Fig. 4. AFM cross section showing the boundary area of a pit electrochemically etched into pure zinc.
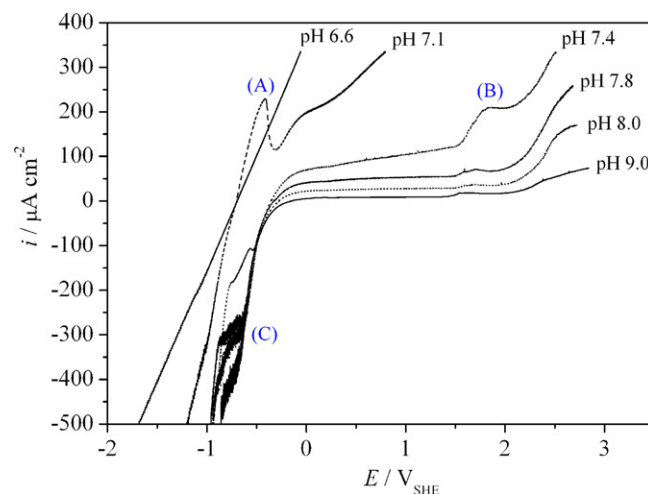
Fig. 6. Potential sweeps (combined anodic and cathodic direction, $2\,mV\,s^{-1}$) of pure zinc in 0.1 M borate buffer at different pH values.
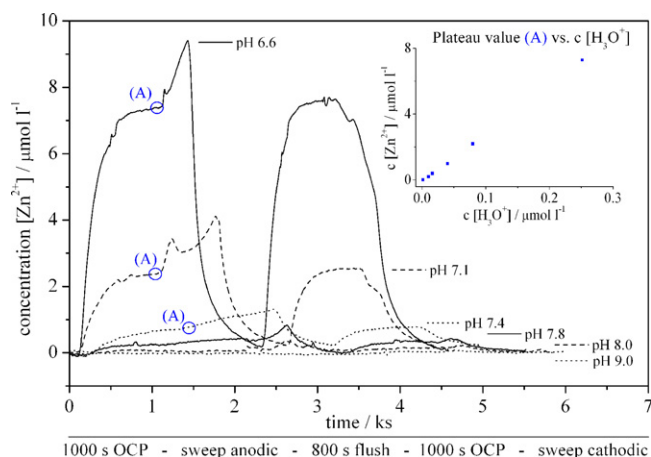
Fig. 7. UV–vis analysis of zinc concentration profiles during potential sweep experiments.

by barrier formation [24]. The absence of this peak on all curves of higher pH shows the presence of the barrier film prior to the sweep, which is in agreement with the analysis of the corrosion potential. However, the passive current density decreases significantly with increasing pH indicating that the passive surface is still very sensitive to minor changes in pH.

The current response to polarisation observed at a pH value of 6.6 is purely resistive which is caused by the low conductivity of undissociated boric acid which contains only small amounts of sodium borate at this pH value.

The increase in current density at high anodic potentials (B) is interpreted as the inhibition of a film breakdown event at the peak position by supersaturation of the interface and repassivation by a precipitation. This effect is known as the growth of Type II oxide [6,25]. The dimension of this additional passivation inversely corresponds to the solubility of zinc in the studied medium.

The cathodic sweep (C) reveals an increasing cathodic current with increasing pH. In no case, a plateau was found for the oxygen reduction reaction [26] which contradicts a purely transport controlled mechanism, even though certain characteristics can be observed. The deviations from transport control are attributed to the presence of a passive layer which is known to interfere with oxygen reduction processes [5].

3.2.3. UV–vis analysis

UV–vis spectrometric quantification of the zinc dissolution was performed in parallel to the measurements shown before. The sequence of measurements and the zinc profile is shown in Fig. 7. All curves show an initial rise to a plateau value (A), followed by a zinc peak caused by anodic dissolution. In the case of pH 7.1, this anodic profile follows the current density observed in the sweep experiment.

After the anodic sweep, the cell is lifted and flushed in air for 800 s. Due to the different time required to reach the dynamic end value of the sweep experiment (longer experiment times are required with longer passivity ranges), the events indicated on the bottom of Fig. 7 are not confined to an absolute time with the exception of the first 1000 s OCP measurement (which starts at $t = 0$ s) and the anodic sweep ($t = 1000$ s). Please note that no correction for t_d is applied.

Subsequently to the first measurement location, a new position on the substrate is approached and the cathodic measurement takes place, leading to a zinc plateau observed before but suppressed by the cathodic polarisation after 1000 s OCP measurement. The reproducibility of the plateau values (A) in the series of a singular pH value can be undoubtfully proven. A noticeable feature is

the homogeneity of zinc etching by the borate buffer, clearly indicating an initiation period and a quick convergence towards the steady state concentration. A plot of the steady state value against the concentration of protons calculated from the pH value gives a linear relation.

The two possible reasons for these increasing zinc signals are a rise in the corrosion current density or an increased dissolution of the passive film formed on the surface. Given the high overpotential of hydrogen on zinc, the cathodic reaction is dominated by the oxygen reduction which is pH dependent to some extent, but primarily transport controlled [25,27,28]. The sole electrochemical steady state between cathodic and anodic reactions on the zinc surface cannot account for the observed phenomena.

Rather than this, the chemical dissolution of the passive film according to

$$ZnO + H^+ \rightarrow [Zn(OH)]^+ \qquad (2)$$

or

$$Zn(OH)_2 + H^+ \rightarrow [Zn(OH)]^+ + H_2O \qquad (3)$$
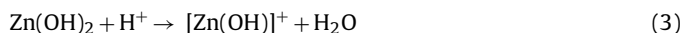
matches the relationship shown. The dissolution of pure ZnO in slightly acidic (pH 4–7) media is diffusion controlled with respect to the proton concentration [29]. The same applies for the protonation of zinc hydroxide [9,23] and therefore accounts for the linear increase in zinc dissolution with proton concentration. The fact that the slope of this linear relation is around 22 originates from the buffer effect where the local depletion of protons is opposed by the reaction of boric acid to the corresponding base. Thus, the availability of protons exceeds the activity of those with the buffer acting as a proton carrier agent.

The observed dissolution kinetics concludes the decomposition reaction of the passive film to be the dominant process regarding the release of zinc into the solution. This implies that a chemical dissolution reaction according to Eqs. (2) and (3) takes place in all conditions presented in this study. Thus, even pH values of 6.6 and 7.1 allow formation of a passive film, even though its integrity is compromised by the quick chemical dissolution reaction preventing the film to provide passive behaviour in the open circuit potential measurements.

This is in agreement with the results obtained by Boto and Williams [5] who observed the inhibition of the oxygen reduction reaction on zinc by hydroxide formation for pH values above 5.2. Even though a general inhibition effect of surface precipitates or oxides on the electrochemical behaviour is obvious, the effect on different electrochemical properties differs significantly. The open circuit potential is clearly dominated by the relation between the rates of oxide formation and dissolution with a precise threshold for the film integrity that ultimately causes an instant shift from active to passive values. The potentiodynamic measurements in contrast reflect the stability of the passive film by the passivity current that qualitatively correlates with the rate of film decomposition (thus, lower dissolution rates yield lower passivity currents). In any case, the electrochemical data presented did at no time allow calculation of the exact rate of zinc dissolution and the mass loss as direct consequence. The real time monitoring of zinc during all experiments therefore provides crucial information on the dominant processes for zinc dissolution that are of chemical rather than electrochemical nature in the experiments presented.

To quantify the relationship between zinc dissolution and measured current density, the concentration profiles are transformed into a corresponding current by taking $z = 2$ for Zn^{2+} in Eq. (1). Fig. 8 shows the OCP-anodic sweep couple in a XY_1Y_2-Plot with the current density calculated from the spectrometric zinc detection (i_{Zn}) and the current density measured by the potentiostat (i) as a function of the measurement time. The experiment sequence is shown on the top of each graph for clarification. It can be seen

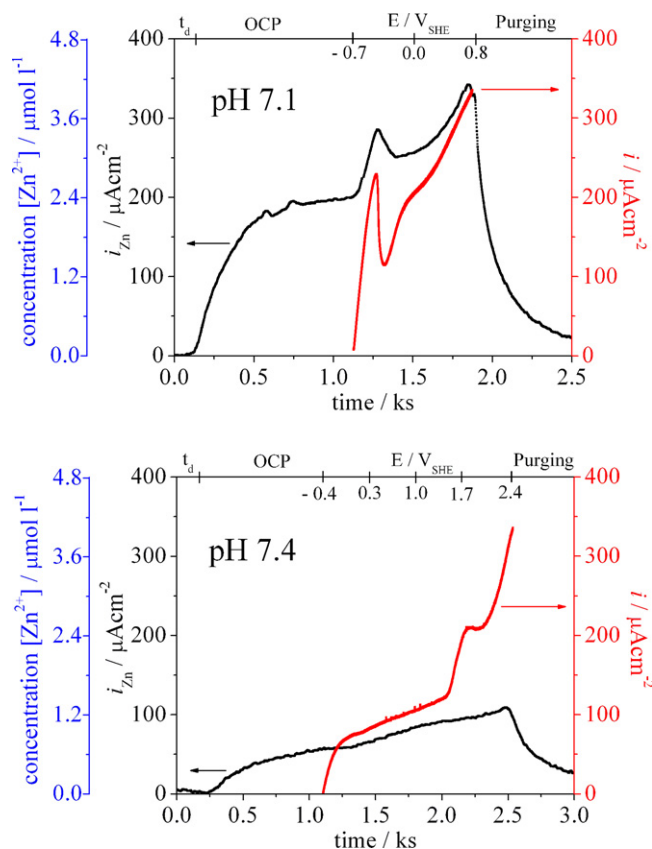**Fig. 8.** Combination of dissolution profiles and current density, the latter being shifted by t_d.

that in the case of pH 7.1, the chemical dissolution of zinc is dominant over the anodic current density ($i_{Zn} > i$) whereas at pH 7.4, an inverse behaviour is observed. In the former case, the chemical dissolution proceeds at very high rates with the polarisation induced dissolution in addition. The latter case indicates an oxidation current without liberation of zinc ions into the solution, which is an expected behaviour for passive film formation. Apparently, a high amount of zinc is either formed as an oxide or precipitates on the surface. This confirms a significant thickening of the passive film during anodization indicating that the film formation by anodic polarisation and the chemical dissolution proceeds at very different rates.

3.3. The effect of sulfate-anions

To further prove the chemical film decomposition to be of dominant importance for the electrochemical behaviour of zinc, sulfate anions were added which are electrochemically inert under the applied potentials, but act as film destabilizing species regarding passive film formation [12]. The recorded corrosion potentials at pH 8.0 and pH 9.0 are shown in Fig. 9. As observed in Fig. 5, both an active and a passive state occur. The transition can be located between 1 and 10 mM Na_2SO_4 in pH 8.0 and between 10 and 100 mM in pH 9.0 respectively. It is obvious that an interference of sulfate ions with the formation of the passive films takes place. It is noteworthy that a penetration model does not apply to corrosion at the rest potential. Moreover, a complexation mechanism with either incorporation of sulfate anions in the film [30] or an increased solubility of zinc at a given pH value [31] seems reasonable. The logarithmic formation constants of zinc–sulfate complexes are comparably high with respect to halide ions and is in direct competition with the formation of hydroxyl-complexes and
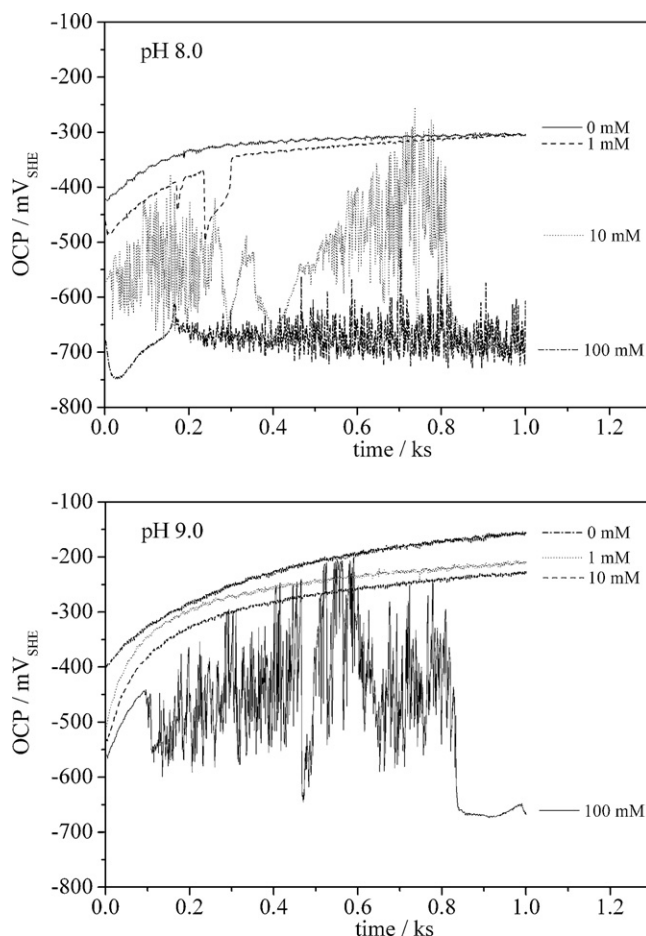

Fig. 9. Development of the open circuit potential of zinc in 0.1 M borate buffer in the presence of different Na_2SO_4 concentrations.
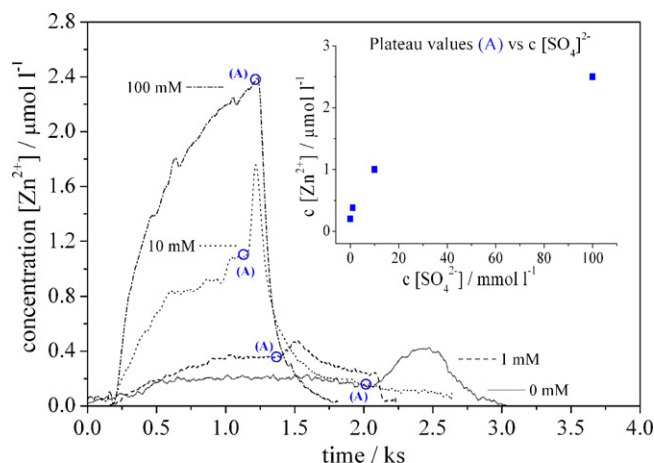

Fig. 10. Zinc dissolution profile at pH 8.0 with different additions of sodium sulfate. Only the anodic sweep after 1000 s OCP is shown.

ligand bridging [32]. In any case, the integrity of the film is lowered with the addition of sulfate ions. If the concentration of these ions falls below a certain threshold allowed by the pH value, the passivity condition is met and a corrosion potential around −300 mV SHE is found. Higher additions lead to active potentials or even frequent alternations (e.g. pH 8.0 in addition with 10 mM sulfate). Potential sweeps performed under these conditions showed pitting [12,25], but lacked in reproducibility of the other measurements presented in this study. However, the correlation between sulfate concen-

tration and pitting potential was negative, thus higher amounts of sulfate caused diminished or vanished periods of passivity. These investigations can be extended to zinc magnesium alloys [33].

The dissolution profile in Fig. 10 supports the aspect of increased solubility and shows the zinc concentration to rise with increasing sulfate concentration following a saturation curve. It should be noted that the measurement with 100 mM sulfate did not exhibit a concentration plateau within 1000 s, therefore the last data point in the derived $c[Zn^{2+}]$ vs. $c[SO_4^{2-}]$ diagram is probably underestimated.

4. Conclusions

The feasibility of a flow type scanning droplet cell with in situ detection via UV–vis to investigate zinc corrosion at the rest potential has been demonstrated. A detection limit around $0.1\,\mu\mathrm{mol\,l^{-1}}$ has been achieved. Critical for this sensitivity is a stable and laminar flow of electrolyte.

The dependency of the open circuit potential of zinc in 0.1 M borate buffer on the pH value has been demonstrated in the presence of convection and in the range of pH 6.6–9.0. A passive and active state was identified with a well localized transition between pH 7.1 and 7.4. Potential sweeps provided additional data on the passivity current density decreasing with increasing pH in a more steady way.

Zinc concentration profiles obtained during the experiments revealed a steady etching process as indicated by a plateau in the concentration diagram during 1000 s OCP measurements. The rate of the dissolution reaction is diffusion controlled at all pH values (6.6–9.0). The fraction of zinc ions liberated by anodic polarisation is in all examined pH values minor to the steady state dissolution process.

Sulfate ions interfere with the passivity of zinc and increase the etching rate at OCP. The pitting potential decreases with increased sulfate concentration. The increase in zinc corrosion can neither be estimated by the OCP nor the potential sweeps. In situ analysis therefore provides essential information for both estimating the corrosion properties and mechanistic considerations.

References

[1] B. Schuhmacher, C. Schwerdt, U. Seyfert, O. Zimmer, Surf. Coat. Technol. 163 (2003) 703.
[2] T.E. Graedel, J. Electrochem. Soc. 136 (1989) C193.
[3] M. Pourbaix, Atlas of Electrochemical Equilibria in Aqueous Solutions, Pergamon, New York, 1966.
[4] T. Hurlen, Acta Chem. Scand. 16 (1962) 1346.
[5] K.G. Boto, L.F.G. Williams, J. Electroanal. Chem. 77 (1977) 1.
[6] R.W. Powers, M.W. Breiter, J. Electrochem. Soc. 116 (1969) 719.
[7] Y.C. Chang, G. Prentice, J. Electrochem. Soc. 136 (1989) 3398.
[8] S. Bonk, M. Wicinski, A.W. Hassel, M. Stratmann, Electrochem. Commun. 6 (2004) 800.
[9] C. Fenster, M. Rohwerder, A.W. Hassel, Mater. Corr. 60 (2009) 855.
[10] L.F.G. Williams, Surf. Technol. 4 (1976) 355.
[11] F.H. Assaf, S.S. Abd El-Rehiem, A.M. Zaky, Mater. Chem. Phys. 58 (1999) 58.
[12] E.E. Abd El Aal, S.A. El Wanees, Corros. Sci. 51 (2009) 1780.
[13] E.E.F. El Sherbini, S.S. Abd El Rehim, Corros. Sci. 42 (2000) 785.
[14] E. Tada, K. Sugawara, H. Kaneko, Electrochim. Acta 49 (2004) 1019.
[15] C.J. Park, M.M. Lohrengel, T. Hamelmann, M. Pilaski, H.S. Kwon, Electrochim. Acta 47 (2002) 3395.
[16] M. Mokaddem, P. Volovitch, K. Ogle, Electrochim. Acta 55 (2010) 7867.
[17] M.M. Lohrengel, C. Rosenkranz, I. Klüppel, A. Moehring, H. Bettermann, B. Van den Bossche, J. Deconinck, Electrochim. Acta 49 (2004) 2863.
[18] A.I. Mardare, A.W. Hassel, Rev. Sci. Instrum. 80 (2009) 046106.
[19] A.W. Hassel, K. Fushimi, M. Seo, Electrochem. Commun. 1 (1999) 180.
[20] K. Ogle, S. Weber, J. Electrochem. Soc. 147 (2000) 1770.
[21] P. Richter, M.I. Toral, A.E. Tapia, E. Fuenzalida, Analyst 122 (1997) 1045.
[22] S.O. Klemm, A.G. Martin, J. Lengsfeld, J.C. Schauer, B. Schuhmacher, A.W. Hassel, Phys. Status Solidi A 207 (2010) 801.
[23] R.A. Reichle, K.G. McCurdy, L.G. Hepler, Can. J. Chem. – Rev. Can. Chim. 53 (1975) 3841.
[24] X.G. Zhang, Corrosion and Electrochemistry of Zinc, Springer, New York, 1996.
[25] R. Hausbrand, M. Stratmann, M. Rohwerder, J. Electrochem. Soc. 155 (2008) C369.
[26] M.B. Liu, G.M. Cook, N.P. Yao, J. Electrochem. Soc. 128 (1981) 1663.
[27] C. Deslouis, M. Duprat, C. Tulettournillon, J. Electroanal. Chem. 181 (1984) 119.
[28] Z. Pilbath, L. Sziraki, Electrochim. Acta 53 (2008) 3218.
[29] J. Guśpiel, W. Riesenkampf, Hydrometallurgy 34 (1993) 203.
[30] E.E. Abd El Aal, Corros. Sci. 42 (2000) 1.
[31] I.M. Kolthoff, T. Kameda, J. Am. Chem. Soc. 53 (1931) 832.
[32] R.J. Brodd, V.E. Leger, Encyclopedia of Electrochemistry of the Elements, Marcel Dekker, New York, 1976.
[33] S.O. Klemm, J.C. Schauer, B. Schuhmacher, A.W. Hassel, Electrochim. Acta, submitted for publication.